

An Experimental Study of Planar Impact of a Robot Manipulator

Prabhakar R. Pagilla and Biao Yu

School of Mechanical and Aerospace Engineering
Oklahoma State University
Stillwater, OK 74078-5016

pagilla@ceat.okstate.edu

Abstract

This paper provides an experimental study of planar impact of a robot manipulator on a surface. Using the data collected from a series of experiments, it investigates post-impact behavior for different pre-impact conditions such as configuration of the robot, angle and velocity of impact, etc. Understanding the post-impact behavior for various pre-impact conditions can result in the design of improved transition control strategies to stabilize the manipulator onto the surface. Potential applications of this study include robotic surface finishing operations such as polishing, chamfering, deburring, and grinding, etc.

1 Introduction

Many robotic applications involve interaction of the robot with its environment. Examples include robotic assembly tasks and robotic surface finishing operations such as deburring, grinding, chamfering, and polishing, etc. In many of these applications the environment is an object to be manipulated or a work piece to be machined by a robot. Contact of a robot with an environment will lead to impact if the robot has non-zero normal velocity component at the point of impact. Modeling the dynamics during impact has received considerable attention in the mechanics literature as well as the robotics literature. Study of the impact phenomenon is essential for a stable operation of robotic contact tasks.

A typical surface finishing operation involves a robot manipulator moving in free space before making contact with the surface to be machined. If the robot end-effector impacts the surface with a non-zero normal velocity then the end-effector has to be stabilized onto the surface before any surface finishing operation can take place. This transition from free motion of the robot to motion on the constrained surface is generally called the transition phase. In the transition phase the robot may experience severe bounces due to impact with the surface. An experimental understanding of the impact phenomena facilitates an efficient design of a stable controller during the transition phase.

Study of impact has been extensive in the mechanics literature [2, 6, 8]. An impact model is chosen to predict the post-impact behavior of the manipulator based on pre-impact conditions. A number of impact models exist in the literature [2, 8, 13, 15]. Central to the impact model is the so called coefficient of restitution. There are three distinct definitions of the coefficient of restitution: (1) kinematic coefficient (Newton's coefficient), defined as the ratio of post-impact to pre-impact normal velocity; (2) kinetic coefficient (Poisson's coefficient), defined as the ratio of post-impact to pre-impact impulse; and (3) energetic coefficient, defined as the ratio of post-impact to pre-impact energy. An extensive discussion of different coefficients of restitution can be found in [2, 14].

Impact of a robot manipulator with an environment has been an active research area; see [17, 5] and the references therein. Impact minimization using redundant degrees of freedom in robots has been considered in [17]. A dimensionless behavior of impact was developed in [18]. An extensive theoretical study of nonsmooth impact mechanics and dynamics and control of impact of a robot can be found in [5] and its bibliography.

The authors prior work has primarily focused on modeling and control design for a complete robot task [9, 10, 11]. An uncertainty in the constraint surface location can cause the robot to impact the surface. Experimental observations of impact have indicated that the post-impact robot behavior varies considerably for different pre-impact conditions. Some observed aspects include a jump in the tangential velocity, and in some cases reversal of tangential velocity component at the point of impact. Further, for some pre-impact conditions, the post-impact tangential velocity may increase. These effects have been qualitatively reported in literature [14], but have been seldom verified experimentally. Different pre-impact conditions and manipulator configurations are considered in this study. Insight from these experiments can facilitate better understanding of the impact behavior and can lead to more efficient controller design for the transition phase in robotics.

The rest of the paper is organized as follows. Section 2 gives the dynamic equations of the robot manipulator and explains the impact phenomena related to the manipulator

dynamics. Experimental procedure and different manipulator configurations are given in section 3. Experimental results for different pre-impact conditions are discussed in section 4. Section 5 gives some conclusions of the paper.

2 Manipulator Impact Dynamics

Consider the schematic of a two-degree-of-freedom planar manipulator and a surface as shown in Figure 1. The joint position vector is denoted by $q \in \mathbb{R}^2$ and the Cartesian position vector by $x \in \mathbb{R}^2$. The forward kinematics map of the manipulator is given by $x = h(q)$, and the velocity kinematics is $\dot{x} = J(q)\dot{q}$, where $J(q)$ is the Jacobian associated with the forward kinematics map. The dynamics of the manipulator is given by

$$M(q)\ddot{q} + C(q, \dot{q})\dot{q} = \tau + J^T(q)f \quad (1)$$

where $M(q)$ is the symmetric positive-definite inertia matrix, $C(q, \dot{q})$ is the matrix composed of Coriolis and centripetal forces, τ is a vector of joint motor torques, f is the vector of contact force. The constraint surface is given by

$$\phi(x(q)) = 0. \quad (2)$$

In the presence of the surface in the workspace of the manipulator, we can divide the state space into the following:

$$X_u = \{q, \dot{q} \in \mathbb{R}^2 : \phi(q) < 0\} \quad (3)$$

$$X_c = \{q, \dot{q} \in \mathbb{R}^2 : \phi(q) = 0\} \quad (4)$$

$$X_f = \{q, \dot{q} \in \mathbb{R}^2 : \phi(q) > 0\} \quad (5)$$

where X_u represents manipulator configurations in which it can freely move, X_c represents configurations where the manipulator lies on the surface, and X_f represents configurations that are not reachable. The set X_c can be further sub-divided into sets X_{ct} and X_{ca} , i.e., $X_c = X_{ct} \cup X_{ca}$, given by

$$X_{ct} = \{q, \dot{q} \in \mathbb{R}^2 : \phi(q) = 0, P_\phi(q)\dot{q} \neq 0\} \quad (6)$$

$$X_{ca} = \{q, \dot{q} \in \mathbb{R}^2 : \phi(q) = 0, P_\phi(q)\dot{q} = 0\} \quad (7)$$

where $P_\phi(q)\dot{q}$ indicates joint velocity component that is normal to the constraint surface, and $P_\phi(q)$ is the orthogonal projection matrix whose image represents the normal direction of the constraint and is given by

$$P_\phi(q) = (\nabla\phi(q))^T(\nabla\phi(q))/\|\nabla\phi(q)\| \quad (8)$$

where $\nabla\phi(q)$ is the gradient of the surface. The motivation for the sub-division of the set X_{ca} is to separate collision conditions from smooth landing of the manipulator on the surface. $P_\phi(q)\dot{q} \neq 0$ at contact leads to impact with the surface. Depending on the pre-impact conditions, the manipulator end-effector may bounce on the surface one or more times. It is essential to stabilize the end-effector onto the surface before performing a surface finishing operation

which involves simultaneous motion and force control of the robot. This transition from free motion of the manipulator to stable contact with the surface is the so called transition phase in robotics. For a detailed description of dynamic modeling of the robot performing surface finishing operations we refer the reader to [9, 10].

Impacts are generally treated as very large forces acting over a short duration of time. If we assume that impact occurs over an infinitesimally small period of time, then (1) all velocities remain finite and (2) there is no change in the position of the system. If $\Delta t \rightarrow 0$ is the duration of collision then the force impulse f_I due to impact at time t_* is

$$f_I = \int_{t_*}^{t_* + \Delta t} f(\omega)d\omega. \quad (9)$$

Integrating (1) from t_* to $t_* + \Delta t$, the dynamics during impact becomes

$$M(q)\sigma_{\dot{q}} = J^T(q)f_I \quad (10)$$

where $\sigma_{\dot{q}} := \dot{q}_+ - \dot{q}_-$, \dot{q}_- and \dot{q}_+ represent pre-impact and post-impact velocities. In the Cartesian coordinates, the change in velocity is given by

$$\sigma_v := J(q)M^{-1}(q)J^T(q)f_I \quad (11)$$

where $v := \dot{x}$ and $\sigma_v := v_+ - v_-$. One method of obtaining post-impact velocities from pre-impact velocities is to assume Newton's restitution model for normal velocity, i.e.,

$$n^T(x)v_+ = -e_n n^T(x)v_- \quad (12)$$

where e_n denotes the normal coefficient of restitution and $n(x)$ is the unit normal vector to the constraint surface. Pre-multiplying (11) by $n^T(x)$ and substituting (12), we obtain

$$-(1 + e_n)n^T(x)v_- = n^T(x)J(q)M^{-1}(q)J^T(q)f_I \quad (13)$$

For an ideal impact there is no change in position of the system, which implies that there is no relative motion between the robot end-effector and the constraint surface during impact. Therefore, there is no friction force, which means that there is no tangential impulse. Hence, the contact force impulse is $f_I = f_{nI}n(x)$ where f_{nI} is the magnitude of the normal impulse. Substituting this into (13) we obtain

$$f_{nI} = -(1 + e_n) \frac{n^T(x)v_-}{n^T(x)H(q)n(x)} \quad (14)$$

where $H(q) = J(q)M^{-1}(q)J^T(q)$. Let $t(x)$ be the unit tangential vector to the constraint surface. Pre-multiplying (11) with $t(x)$ and using (14) we obtain

$$t^T(x)\sigma_v = t^T(x)H(q)n(x)f_{nI} \quad (15)$$

Substituting (14) into (15) we obtain

$$t^T v_+ = t^T(x)v_- - \frac{t^T(x)H(q)n(x)}{n^T(x)H(q)n(x)}(1 + e_n)n^T(x)v_- \quad (16)$$

This above equation gives the post-impact tangential velocity. Equation (16) together with (12) give the post-impact velocity knowing the coefficient of restitution. Notice that even though we assumed that the tangential impulse is zero, we still have a jump in the tangential velocity given by (16). This jump is primarily due to the configuration of the robot. From (16), we can observe that the sign of $t^T(x)H(q)n(x)$ determines the sign of the jump in the tangential velocity.

For a non-ideal impact, the contact force impulse, f_I , generally has components both in the normal and tangential directions. The contact force impulse can be expressed as $f_I = f_{nI}n(x) + f_{tI}t(x)$, where f_{nI} and f_{tI} are the magnitude of the normal force impulse and tangential force impulse, respectively. For this non-ideal case of f_I , we require another equation in addition to (12) and (11) to get post-impact behavior, i.e., compute f_{nI} , f_{tI} and the post-impact tangential velocity. This additional equation can be obtained by assuming the existence of the kinetic coefficient of restitution[2], that is the ratio of the tangential to normal force impulse. Even though in the non-ideal case there is a component of the contact force impulse in the tangential direction, but this is small compared to the normal component. This is in fact validated by our experimental results, which are shown in the following sections.

3 Experimental Platform

The complete experimental platform used in all experiments is shown in Figure 1. The main part of this experimental platform is a two-axis direct drive manipulator as shown in Figure 1. Each axis is driven by an NSK Megatorque direct drive servo-motor which is capable of up to 3 revolutions per second maximum velocity and position feedback resolution of upto 156,400 counts per revolution. The end of link 2 of the manipulator contains a force sensor and an end-effector as shown in Figure 1. The end-effector is fixed to the force sensor, and is a simple assembly consisting of a circular plate and a metal probe. In robotic surface finishing experiments the end-effector is replaced by a deburring tool assembly and the probe becomes a cutting or polishing tool. A mechanical vice firmly holds a thick aluminum piece, which acts as the constraint surface.

3.1 Experimental Procedure

The experimental procedure consists of the manipulator moving towards the surface at a certain impact angle and making contact with the surface. The procedure involves maintaining a prescribed velocity of the end-effector and the angle of impact using the motor torques. Just prior to the end-effector impacting the surface the motor torques are shut-off to mimic free impact with a prescribed velocity and angle. Joint angles, joint velocities and force on the end-effector are collected every four milli-seconds. The

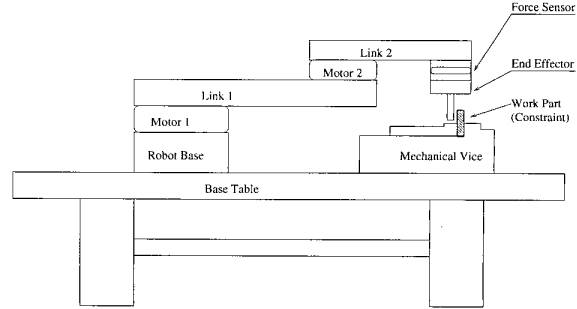


Figure 1: Manipulator and the constraint fixture

two manipulator configurations, i.e., up-elbow and down-elbow, are shown in Figures 2 and 3, respectively, where α represents the angle of impact. For each configuration we consider three velocities of impact (0.1 m/s, 0.2 m/s, and 0.3 m/s) and four different angles of impact (30 deg., 45 deg., 60 deg., and 90 deg.). Impact velocities larger than 0.3 m/s were not tried as the impact force exceeds the force sensor safety limit.

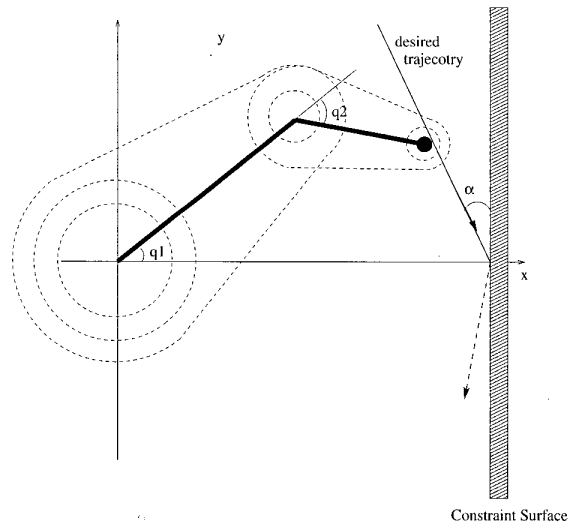


Figure 2: Up-elbow configuration

4 Experimental Results

The normal and tangential velocity profile of the end-effector for an impact velocity of 0.2 m/s and different angles of impact are shown in Figures 4 and 5 for up and down-elbow configurations, respectively. Notice that there is a jump in the normal and tangential velocity components at impact. For different manipulator configurations, it is interesting to observe that the tangential velocity component may increase in magnitude and/or reverse its direction after im-

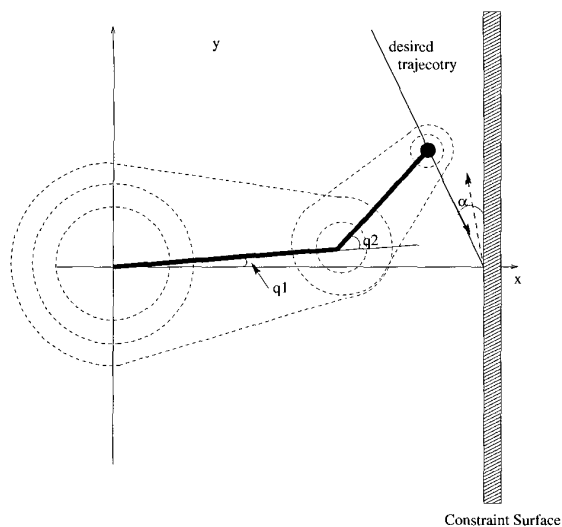


Figure 3: Down-elbow configuration

pact. Further, the tangential velocity jump increases with increase in the angle of impact.

Figures 6 and 7 show the tangential and normal impact force magnitude near the impact for up-elbow and down-elbow conditions. Notice that the time axis interval is only of 0.2 seconds duration. The normal and tangential impact forces shown in the figure are forces on the robot as recorded by the force sensor. For both up-elbow and down-elbow configurations the normal and tangential impact forces increase with increase in the impact angle. Observe that the tangential impact force for up-elbow configuration is in different direction to that of the down-elbow configuration, which is consistent with the tangential velocity jump. Also, notice that the tangential impact force is around 10 percent or less of the normal impact force, which validates the assumption made in section 2 that the normal force impulse dominates the tangential force impulse.

The robot path in the Cartesian space near impact is shown in Figures 8 and 9 for up-elbow and down-elbow configurations, respectively. The dashed lines in the figures represents the constraint surface and the solid line represents the robot path. Figure 8 shows that the angle of departure of the end-effector is different than the angle of impact. This would mean that the post-impact tangential velocity may increase in magnitude for the up-elbow configuration. Notice that there is a reversal in direction of the robot end-effector for the down-elbow configuration for angles of impact greater than 45 degrees. Further, observe that the robot end-effector tip appears to go into the surface, which is due to the overall compliance of the end-effector and the surface.

Figure 10 shows the kinetic energy profile of the manipulator during impact for up-elbow configuration with impact velocity 0.2 m/s and various impact angles. The kinetic en-

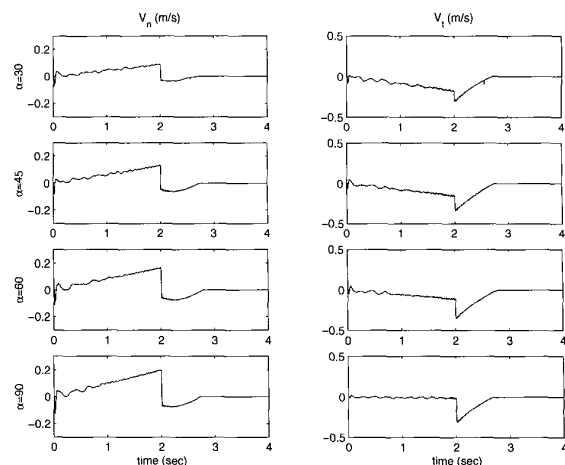


Figure 4: Normal and tangential velocity, $v = 0.2m/s$, up-elbow

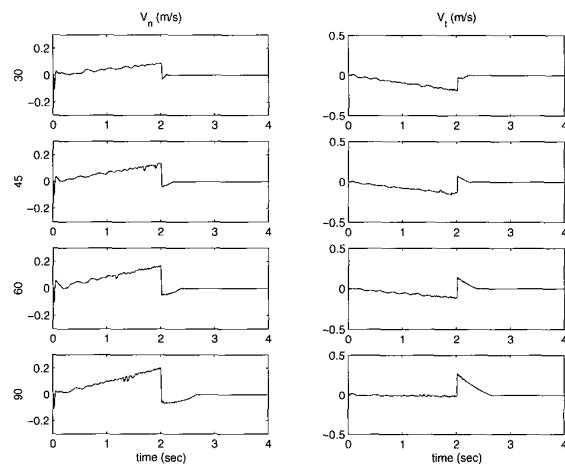


Figure 5: Normal and tangential velocity, $v = 0.2m/s$, down-elbow

ergy drops after impact; and a larger kinetic energy drop can be noticed with increase in the impact angle. Similar post-impact behavior is observed for impact velocities of 0.1 m/s and 0.3 m/s. The results of these experiments were not shown due to lack of space. Figures 11 and 12 give a summary of the ratio of drop in the manipulator kinetic energy during impact to the pre-impact kinetic energy for various conditions. The ratio of drop in manipulator kinetic energy is computed as follows:

$$\text{KE drop ratio} = \frac{\dot{q}_+^T M(q) \dot{q}_+ - \dot{q}_-^T M(q) \dot{q}_-}{\dot{q}_-^T M(q) \dot{q}_-} \quad (17)$$

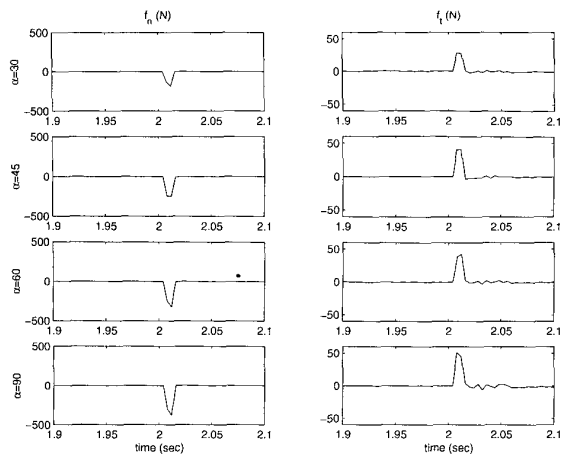


Figure 6: Normal and tangential impact force, $v = 0.2m/s$, up-elbow

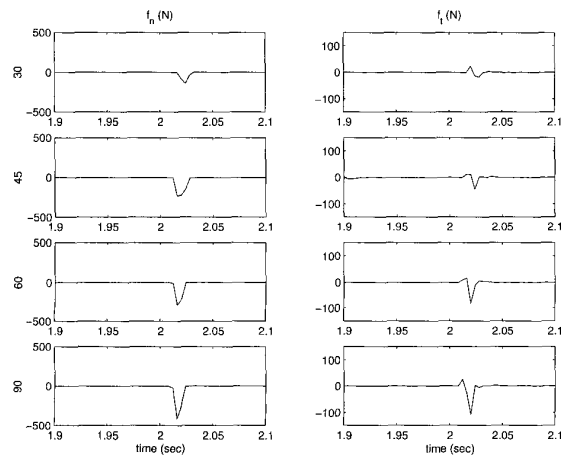


Figure 7: Normal and tangential impact force, $v = 0.2m/s$, down-elbow

5 Conclusions

In this paper, an experimental study was conducted to investigate the post-impact behavior for various pre-impact conditions. This study provides some useful information for designing controllers for the transition phase in robotics. In our previous work [9, 10], we had designed the transition controller with a primary motivation that stable convergence of the end-effector onto the surface should be achieved. The control goal during the transition phase was to drive the end-effector velocity normal to the surface to zero. Factors such as the increase in the magnitude of the tangential velocity and its direction reversal can cause severe problems during the transition phase. The control design in transition phase should take these into account when they occur. Our future work in the design of the transition

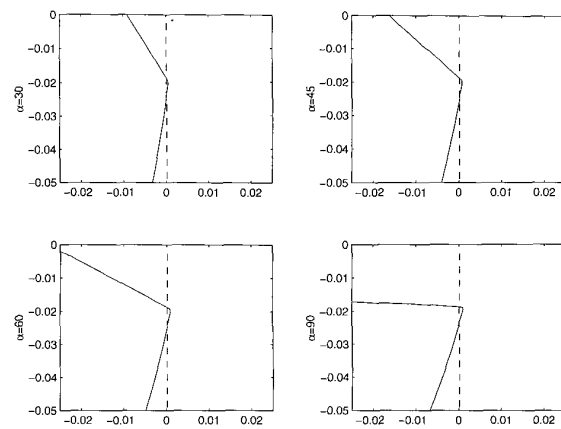


Figure 8: Robot path in Cartesian space near impact, $v = 0.2m/s$, up-elbow

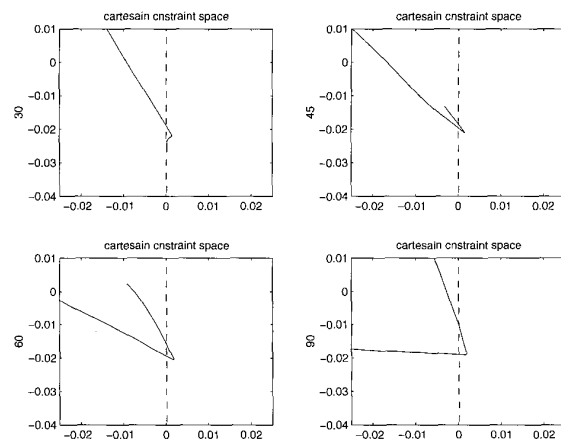


Figure 9: Robot path in Cartesian space near impact, $v = 0.2m/s$, down-elbow

controller will focus on introducing robustness to discontinuous velocity in both normal and tangential direction. To our best knowledge, most research in contact transition control literature has not considered the discontinuous behavior of post-impact tangential velocity. Also, there is a need for general closed-form conditions on the manipulator Jacobian under which the post-impact tangential velocity magnitude can increase and/or reverse direction.

References

- [1] S. Arimoto, *Control theory of non-linear mechanical systems – a passivity-based and circuit-theoretic approach*, Oxford Univ. Press Inc., NY, 1996.
- [2] R.M. Brach, *Mechanical Impact Dynamics: Rigid Body Collisions*, John Wiley & Sons, New York, 1991.

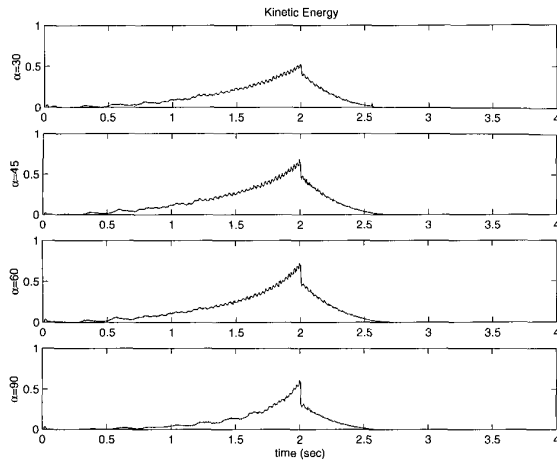


Figure 10: Robot kinetic energy, $v = 0.2m/s$, up elbow

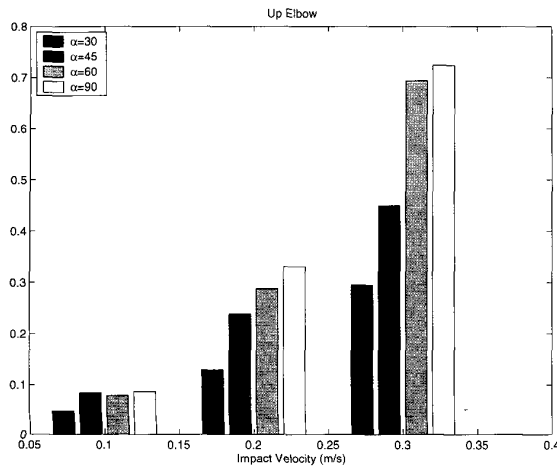


Figure 11: Kinetic energy change during impact, up elbow

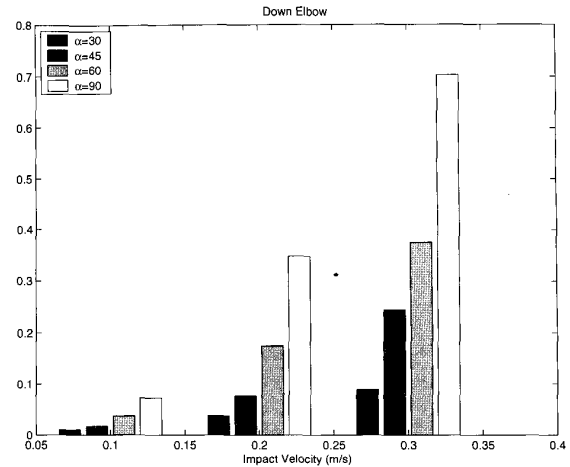


Figure 12: Kinetic energy change during impact, down elbow

[3] R.M. Brach, "Classical Planar Impact Theory and the Tip Impact of a Slender Rod," *Int. J. Impact Engg.*, vol. 13, No. 1, pp. 21–33, 1993.

[4] R.M. Brach, "Predicting Rebound using Rigid Body Dynamics," *ASME Journal of Applied Mechanics*, vol. 59, pp. 700–706, 1992.

[5] B. Brogliato, *Nonsmooth Impact Mechanics: Models, Dynamics and Control*, Springer-Verlag, London, 1996.

[6] W. Goldsmith, *Impact: The Theory and Physical Behaviour of Colliding Solids*, Edward Arnold Publishers, 1960.

[7] J.B. Keller, "Impact with Friction," *ASME Journal of Applied Mechanics*, vol. 53, pp. 1–4, 1985.

[8] V.V. Kozlov and D.V. Treshcev, *Billiards: A Genetic Introduction to the Dynamics of Systems with Impacts*, AMS Translations of Mathematical Monographs, vol. 89, Providence, RI, 1991.

[9] P.R. Pagilla and B. Yu, "Design and Experimental Evaluation of a Stable Transition Controller for Constrained

Robots," Proc. of the IEEE Intl. Conf. on Robotics and Automation, San Francisco, CA, April 2000.

[10] P.R. Pagilla and B. Yu, "A Stable Transition Controller for Constrained Robots," to appear in the IEEE/ASME Trans. on Mechatronics, 2001.

[11] P.R. Pagilla and M. Tomizuka, "Contact Transition Control of Nonlinear Subject to a Unilateral Constraint," *ASME Journal of Dynamic Systems, Measurement, and Control*, Vol. 119, pp. 749–759, 1997.

[12] R.M. Rosenberg, *Analytical Dynamics of Discrete Systems*, Plenum Press, New York, 1977.

[13] C.E. Smith, "Predicting Rebounds Using Rigid Body Dynamics," *ASME Journal of Applied Mechanics*, vol. 58, pp. 754–758, 1991.

[14] C.E. Smith and P. Liu, "Coefficients of Restitution," *Journal of Applied Mechanics*, vol. 59, pp. 963–969, 1992.

[15] W.J. Stronge, "Rigid Body Collisions with Friction," *Proc. of Royal Society of London*, vol. A431, pp. 169–181, 1990.

[16] A. Tornambe, "Modeling and Control of Impact in Mechanical Systems: Theory and Experimental Results," *IEEE Trans. on Automatic Control*, vol. 44, no. 2, pp. 294–309, 1999.

[17] I.D. Walker, "Impact Configurations and Measures for Kinetically Redundant and Multiple Armed Robot Systems," *IEEE Trans. on Robotics and Automation*, vol. 10, no. 5, pp. 670–683, 1994.

[18] K. Youcef-Toumi and D.A. Gutz, "Impact and Force Control: Modeling and Experiments," *ASME Journal of Dynamic Systems, Measurement, and Control*, vol. 16, pp. 89–98, 1994.